e-ISSN: 2687-6698 **Research Article**

Turkish Journal of Analytical Chemistry
www.turkjac.org
2019
TurkJAC

Highly efficient hexavalent chromium removal using *nano*-Fe_3O_4/pomegranate peel biochar/alginate composite as an advanced biosorbent*

Şerife Parlayıcı, Erol Pehlivan**

Konya Technical University, Faculty of Engineering and Natural Science, Department of Chemical Engineering, 42250, Selçuklu- Konya, Türkiye

Abstract

In this study, a novel composite – *nano*-Fe_3O_4/pomegranate peel biochar/alginate hydrogel beads (*n*Fe_3O_4-PPBC/Alg) – was synthesized as an alternative adsorbent for removing Cr(VI) ions from aqueous solutions. The adsorbent material was characterized using FT-IR analysis and scanning electron microscopy (SEM). Cr(VI) removal efficiencies were calculated using the standard batch adsorption method to determine the optimal pH, adsorbent dose, contact time, and initial concentration. Various adsorption isotherms, such as Freundlich, Langmuir, and Dubinin–Radushkevich, were employed to describe the adsorption behavior at equilibrium. The Langmuir adsorption isotherm was found to be the most suitable to describe the observed adsorption phenomena, and the adsorption capacity of *n*Fe_3O_4-PPBC/Alg for Cr(VI) was determined to be 316.25 mg/g by the Scatchard linearization method. To investigate the adsorption processes on the *n*Fe_3O_4-PPBC/Alg, kinetic models, including pseudo-first order and pseudo-second-order models, were applied. The pseudo-second-order kinetic model provided the best fit to the experimental data. The adsorption capacity of pomegranate peel biochar for removing Cr(VI) ions has not been previously enhanced by encapsulating it in an alginate matrix and simultaneously magnetizing it. In this context, this study makes a significant contribution to the existing literature. This research demonstrated that *n*Fe_3O_4-PPBC/Alg is an effective adsorbent for the removal of Cr(VI) from aqueous solutions.

Keywords: Alginate; biochar; Cr(VI); kinetics; *nano*-Fe_3O_4; pomegranate peel

1. Introduction

Although heavy metals are naturally present in the Earth's crust, their concentrations in the environment can become hazardous due to both natural and human-induced processes. Human activities such as mining, agriculture, urbanization, industrial operations, and improper waste disposal are the primary drivers of environmental contamination. These activities significantly accelerate the release and distribution of heavy metals, leading to elevated levels in water which threaten ecological systems and human health. Key industrial sources for the heavy metals include metal processing in refineries, leather tanning, coal combustion in power plants, petroleum combustion in nuclear power facilities, as well as production in plastics, textiles, and microelectronics manufacturing [1]. Chromium is frequently present in industrial wastewater, especially from industries such as catalyst production, electroplating, dye and pigment manufacturing, leather tanning, ceramics, glass production, wood preservation, cooling tower water treatment, corrosion prevention, and alloy manufacturing [2]. The extensive industrial application of chromium has a significant downside: environmental pollution [3,4].

Hexavalent chromium, Cr(VI), is a dangerous and cancer-causing contaminant that presents serious threats to human health and the environment. Many natural water bodies have been contaminated with Cr(VI), a compound known to cause teratogenic, mutagenic, carcinogenic effects, and damage to multiple organs upon human exposure. Consequently, developing an effective and holistic approach for the degradation of Cr(VI) has become crucial, as its high solubility in water and environmental persistence make it a significant global concern. Chromium mainly exists in two forms: Cr(III) and Cr(VI), with Cr(VI) being 100 times more toxic than Cr(III) in aqueous environments. Cr(VI) is primarily present as $Cr_2O_7^{2-}$, CrO_4^{2-}, $HCrO_4^-$ in water [5].

These anions exhibit strong oxidative and migratory properties, posing significant environmental and health risks.

Citation: Ş. Parlayıcı, E. Pehlivan, Highly efficient hexavalent chromium removal using *nano*-Fe_3O_4/pomegranate peel biochar/alginate composite as an advanced biosorbent, Turk J Anal Chem, 7(1), 2025, 22–32.

****Author of correspondence** erolpehlivan@gmail.com
Tel: +90 (332) 205 18 45 **Fax:** N/A
Received: December 4, 2024 **Accepted:** January 19, 2025
https://doi.org/10.51435/turkjac.1595052

**This paper was presented at the 6th International Environmental Chemistry Congress, EnviroChem 05-08 November 2024, Trabzon Türkiye.*

Various methods are available to reduce Cr(VI) concentrations in water bodies, including adsorption [6,7], electrochemical techniques [8], membrane treatments [9], bioremediation [10], chemical precipitation, ion exchange, and reverse osmosis are often expensive, complicated, and ineffective, particularly at low concentrations.

Therefore, there is a pressing need for more cost-effective, eco-friendly, and efficient solutions. Adsorption is favored for its simplicity and broad applicability, making it a competitive technology for addressing heavy metal pollution in water. Various adsorbents, including biopolymer composite [11], activated carbon [12], biochar [13], and modified chitosan [14], have been explored for Cr(VI) removal. Nevertheless, there remains a demand for adsorbents that are more sustainable, environmentally friendly, and cost-effective.

Common adsorbents like biochar, activated carbon, graphene, clays, carbon nanotubes, and organic frameworks are typically nanoscale powders, often modified with metallic or organic materials. However, there remains a need to develop suitable embedding materials to immobilize these nanomaterials within appropriate matrices effectively. Among these materials, activated carbon stands out as the most suitable adsorbent due to its high surface area and excellent adsorption capacity. However, the high cost of commercial activated carbon has driven the search for more affordable alternatives with comparable properties. Among the materials studied, biochar has emerged as one of the most environmentally friendly and functional options. Biochar differs significantly from activated carbon. Its production involves lower temperatures compared to those used for activated carbon. In the case of activated carbon, the biomass undergoes significant carbonization, losing most of its functional groups. To enhance the carbonized surface and increase porosity, it is further treated with steam or chemicals. In contrast, biochar production does not require such treatments. The biomass is carbonized at lower temperatures, preserving its functional groups or even activating them, making biochar a versatile material for various applications.

Biochar has recently gained considerable attention as an effective adsorbent due to its large specific surface area (SSA), abundance of functional groups (FGs), and complex pore structures [15]. Biochar, a carbon-rich material created through the pyrolysis of biomass, has emerged as an affordable, environmentally friendly solution for wastewater contaminant removal [11]. Its appeal lies in its high surface area, rich functional groups, and sustainable production process. However, its slow adsorption kinetics and limited adsorption capacity underscore the need for composite materials with enhanced properties. $HCrO_4^-$ ions can be adsorbed onto the COOH, and OH surface groups of biochar, where they form hydrogen bonds and undergo redox reactions with phenolic compounds. This process facilitates the reduction of Cr(VI) to Cr(III), which is then immobilized in situ on the adsorbent surface.

Numerous studies have previously focused on modifying biochar with nanomaterials or metal nano-oxides [16]. Among these, nano-zero valent iron (*n*ZVI) stands out for its advantageous properties, including low cost, high specific surface area, excellent reducibility, strong reactivity, and nano-scale particle size. Consequently, there is a growing body of research employing *n*ZVI-modified biochar for the remediation of heavy metals and organic pollutants in the environment. This research involves a novel and effective strategy that combines alginate and Fe_3O_4 nanoparticles with biochar derived from pomegranate peel. The *n*Fe_3O_4-PPBC/Alg is a new composite that combines the biocompatibility of alginate, the adsorption capabilities of biochar made from pomegranate peel, and the magnetic properties of Fe_3O_4 nanoparticles. This composite efficiently adsorbs and removes Cr(VI), addressing environmental issues including water pollution. Its cost-effectiveness is increased by its magnetic qualities, which make recovery and reuse simple.

Alginate (Alg) is an inexpensive and easily produced biomaterial rich in carboxyl groups. Alg is a commonly used natural linear anionic polysaccharide, mainly composed of β-1,4-glycosidic linkages between α-L-mannuronic acid and β-D-guluronic acid. It is highly biocompatible, biodegradable, and capable of forming gels of various sizes and shapes through cross-linking with divalent or trivalent metal ions [17]. Alg, a natural polysaccharide extracted from brown algae, is highly regarded for its exceptional gel-forming properties and strong metal ion-binding capabilities. Its biocompatibility, biodegradability, and versatile gel-forming characteristics have made it a popular choice in numerous applications [15]. Because alg has both hydrophilic and hydrophobic groups, it can hold onto a large amount of bound water while being prepared, creating free diffusion routes for molecules that are soluble in water. Alg is a useful substance for treating heavy metal ions because of this characteristic, which permits contaminants to enter the gel's interior. When incorporated into biochar composites, Alg improves adsorption capacity by offering additional binding sites on the composite [18,19].

Expanding on these ideas, Alg and biochar were thoroughly mixed and introduced into a *n*Fe_3O_4 solution, forming a *n*Fe_3O_4-PPBC/Alg composite gel. *n*Fe_3O_4 is highly prone to oxidation and loss, making it

challenging to directly use nano-iron/carbon composite materials [20]. Anaerobic or protective nano-iron can be applied to solve this issue, such as in groundwater environments, beneath an FeS layer, or incorporated into polymers like alginate, chitosan, or polyaniline. Alg, known for its excellent stability and high mechanical strength, is a well-established coating material [21].

This study introduces nFe$_3$O$_4$-PPBC/Alg, a highly effective composite material for enhancing the adsorption of Cr(VI) from aqueous solutions. Using biomass waste as a raw material to produce biochar adsorbents is crucial for reducing the cost of adsorbents. Biochar is favored for its high specific surface area and porosity, which provide abundant adsorption sites. However, most biochars are in powder form, which presents challenges in usage, particularly with complex recovery processes. Magnetic metal oxides such as Fe$_3$O$_4$ have become increasingly popular in recent years. When nano Fe$_3$O$_4$ is incorporated into the adsorbent structure, the composite can be easily separated from the solution medium using an external magnetic field. On the other hand, nano Fe$_3$O$_4$ particles often require combinations with other materials to mitigate issues related to their limited adsorption capacity, powder accumulation, and to enhance their adsorption properties. In light of these factors, nFe$_3$O$_4$-PPBC/Alg was synthesized.

By leveraging the binding properties of Alg, the porous structure of pomegranate peel biochar, and the synergistic effects of Fe$_3$O$_4$ nanoparticles, the composite demonstrates significant potential for adsorption of Cr(VI) in prepared aqueous solutions. The research aims to investigate the factors influencing Cr(VI) adsorption onto nFe$_3$O$_4$-PPBC/Alg, evaluate its adsorption performance using adsorption models, and uncover the underlying mechanisms through FT-IR, and SEM analyses. The uniqueness of this study lies in the fact that Cr (VI) adsorption on nFe$_3$O$_4$-PPBC/Alg has not been reported in the literature. The use of pomegranate peels, derived from plant waste, converted into biochar and encapsulated in non-toxic biopolymers like alginate, presents several advantages over other adsorbents by eliminating the need for complex pre-treatment processes. Utilizing pomegranate peel waste as a raw material helps reduce the challenges associated with waste accumulation. Furthermore, the novelty of this study is emphasized by the use of renewable, low-cost materials, the simplicity of preparation and application, and the enhancement of the alginate gel adsorbent's performance without requiring active chemical processes. Additionally, the system simplifies the removal process by converting the adsorbents into a magnetic form, facilitating their separation from the aqueous medium.

The study evaluates adsorption capacity, kinetics, and Cr(VI) removal mechanisms, providing valuable insights into the composite's efficiency. This offers a cost-effective and promising solution for mitigating Cr(VI) pollution in wastewater, supporting environmental remediation and safeguarding aquatic ecosystems.

2. Material and method

2.1. Preparation of adsorbents

Pomegranates were sourced from a local market in Turkey. The peels and edible parts of the fruit were separated. The peels were washed with pure water and dried in an oven for 24 hours. The dried peels were then heated at 600 °C in a Magma THERM MT1210/B2 muffle furnace for 3 hours under low-oxygen conditions to produce biochar [22]. The biochar (PPBC) was cooled in

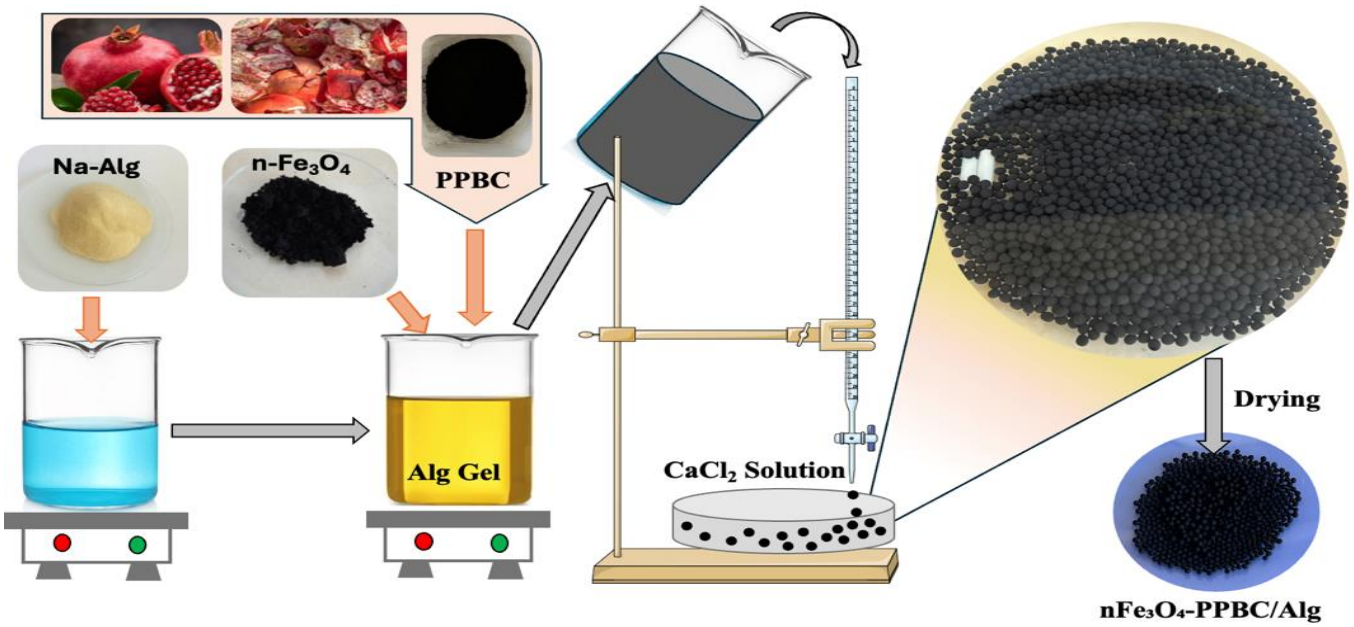

Figure 1. Synthesis scheme of nFe$_3$O$_4$-PPBC/Alg composite

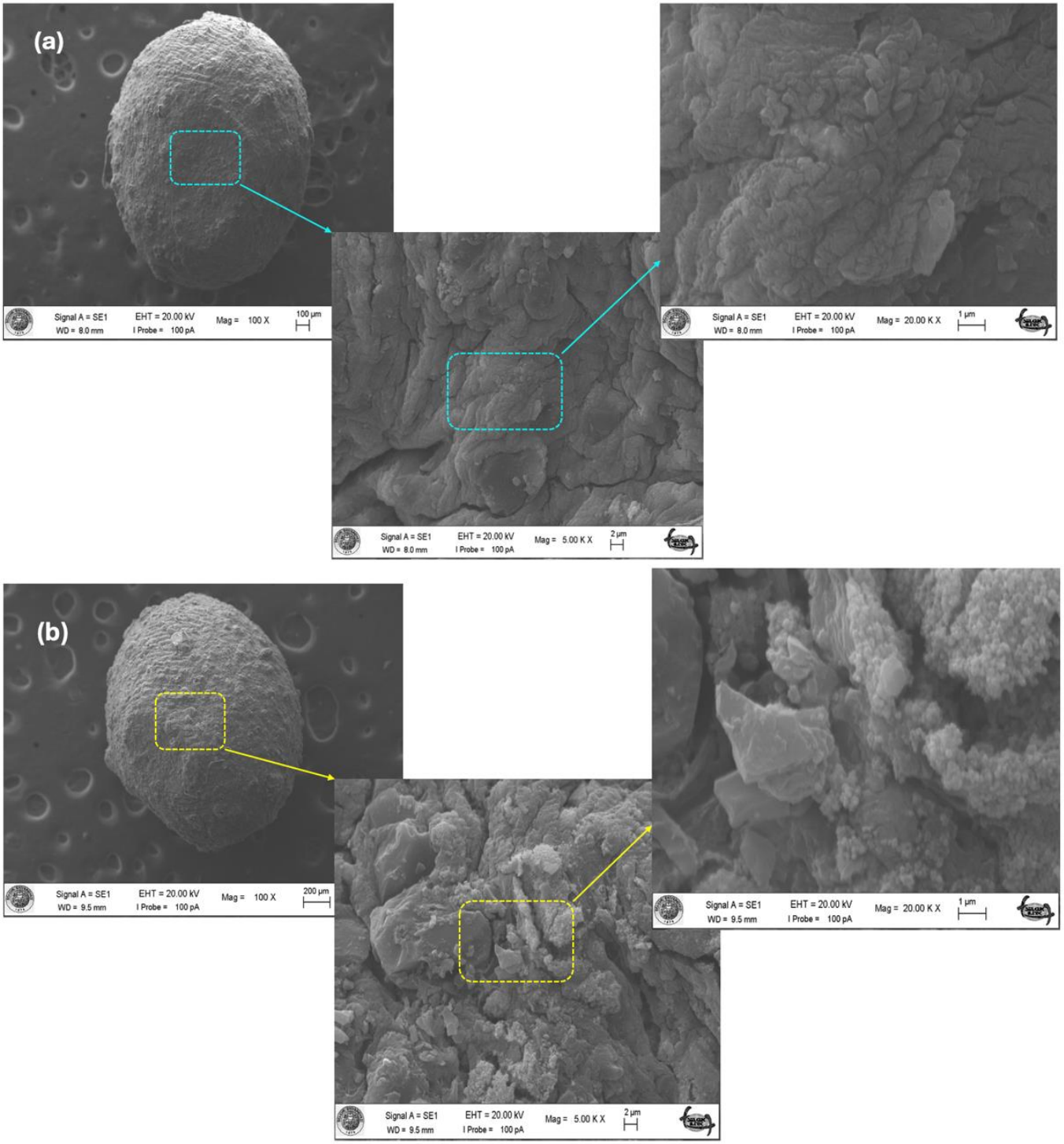

Figure 2. (a) SEM images of *n*Fe_3O_4-PPBC/Algae composite and (b) after adsorption Cr(VI)

a desiccator, ground into a fine powder, and sieved to obtain particles with a size of 125 µm for use in composite preparation. To prepare *n*Fe_3O_4-PPBC/Alg, sodium alginate was first dissolved in 100 ml of distilled water (5% w/v). The solution was mixed with a magnetic stirrer for about 4 hours to create a homogeneous gel. Separately, two suspensions were prepared: one containing 2.5 g of *nano*-Fe_3O_4 in 20 ml of distilled water and another containing 2.5 g of PPBC in 20 ml of distilled water. Each suspension was stirred at 300 rpm for 2 hours to ensure proper dispersion. These suspensions were then added to the alginate gel and stirred with a magnetic stirrer for 6 hours to form a uniform solution. The resulting mixture was introduced dropwise into a 0.5 M $CaCl_2$ solution using a syringe, forming spheres. These spheres (beads) were stirred in the solution at 100 rpm for approximately 3 hours. The beads were left in the solution overnight, then collected by filtration, washed with water until reaching a neutral pH, and dried at 60 °C for 24 hours (Fig. 1). This description details the step-by-step process of preparing the pomegranate peel biochar composite and its incorporation with alginate and iron oxide nanoparticles.

3. Results and discussion

3.1. Characterization of composite

The composite, nFe$_3$O$_4$-PPBC/Alg, was characterized using FT-IR spectroscopy to identify its surface functional groups. Post-adsorption FT-IR analysis was also performed to verify the adsorption of Cr(VI) ions. Surface morphology was studied by capturing scanning electron microscopy (SEM) images of the composite both before and after the adsorption process.

3.2. SEM analysis of composite

Using SEM, the structural differences in nFe$_3$O$_4$-PPBC/Alg before and after Cr(VI) adsorption were observed. The SEM image in Fig. 2a reveals a rough surface before adsorption. In contrast, Fig. 2b shows the Cr (VI) ions forming deposits and accumulating over the surface pores, confirming their successful adsorption onto nFe$_3$O$_4$-PPBC/Alg.

3.3. FT-IR spectrum of composite

The functional groups' types were analyzed using FT-IR spectroscopy. Fig. 3 presents the FT-IR spectra of nFe$_3$O$_4$-PPBC/Alg composite both before and after the adsorption process. From the spectrum, a broad peak around 3270 cm^{-1} indicates the stretching vibrations of O–H groups. The peak at 1590 cm^{-1} corresponds to the stretching vibrations of the carboxyl group (–C=O). A peak at 1420 cm^{-1} is attributed to the stretching vibrations of aromatic C=C bonds. The band observed at 1016 cm^{-1} signifies the stretching of ether (–C–O) and alcohol (–C–O) groups. Additionally, the absorption band at 535 cm^{-1}, characteristic of Fe$_3$O$_4$ nanoparticles, is associated with the Fe–O bond's stretching vibrations.

The surface functional components of nFe$_3$O$_4$-PPBC/Alg after contact with Cr(VI) ions were determined by FT-IR spectrometry. The results are given in Fig. 3. After the removal of Cr (VI) from aqueous media using the nFe$_3$O$_4$-PPBC/Alg composite, the range of absorption peaks in the structure of the produced composite was changed, which could be due to the interaction of present functional groups in the structure of the composite with Cr(VI) ions.

3.4. Effect of solution pH on Cr(VI) adsorption

The pH of a solution plays a critical role in regulating the adsorption process. To examine how pH influences the adsorption of Cr(VI) ions by nFe$_3$O$_4$-PPBC/Alg, the equilibrium concentrations were analyzed at pH levels ranging from 2 to 8, after a 60-minute equilibrium period. These findings are illustrated in Fig. 4. Generally, as the pH increases, the efficiency of Cr(VI) removal by nFe$_3$O$_4$-PPBC/Alg decreases.

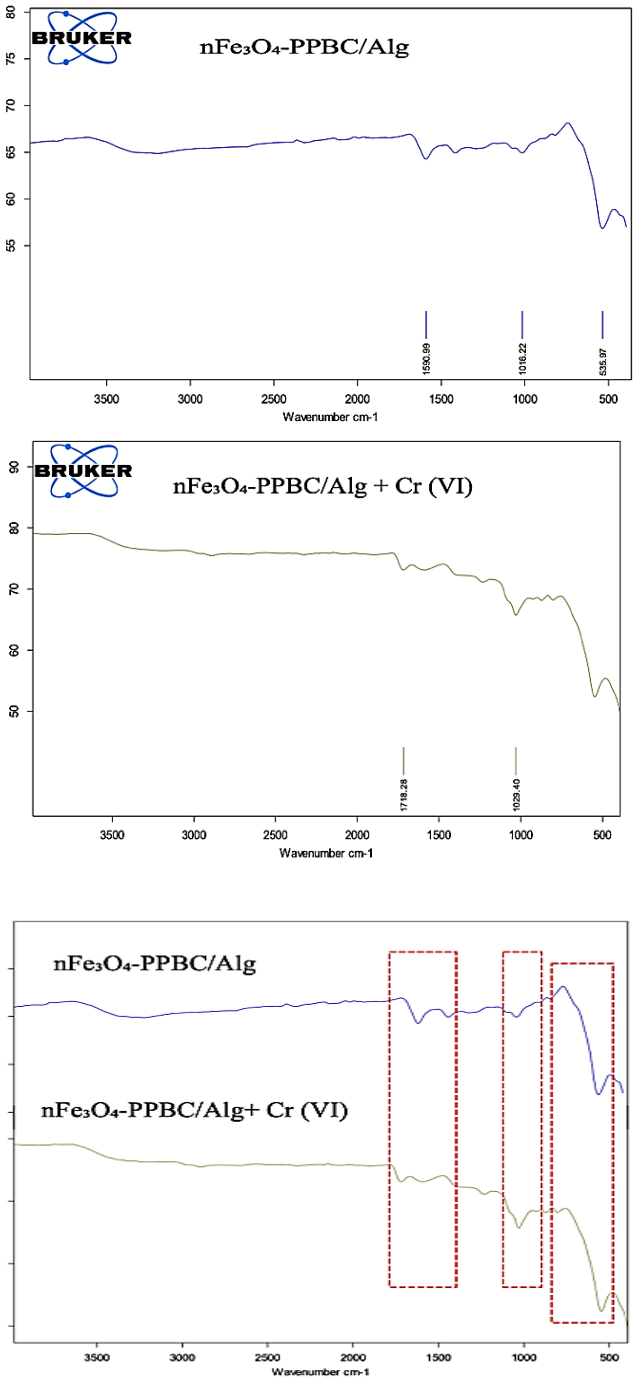

Figure 3. Pre- and post-adsorption FT-IR plot of nFe$_3$O$_4$-PPBC/Algae before and after adsorption

The highest adsorption occurs within the pH range of 2.0 to 3.0. At lower pH levels, the adsorbent surface acquires more positive charges, enhancing the electrostatic attraction for anionic Cr(VI) species [11]. At higher solution pH values, hydroxide ions (–OH) may compete with Cr(VI) for adsorption sites, reducing overall removal efficiency. Venkatrajan et al. reported similar findings, suggesting that the adsorption of Cr(VI) ions is predominantly driven by electrostatic interactions at lower pH levels [5]. The maximum chromium removal efficiency was observed when the adsorbent surface acquired a positive charge through protonation, facilitated by the higher concentration of H$^+$ ions in the medium.

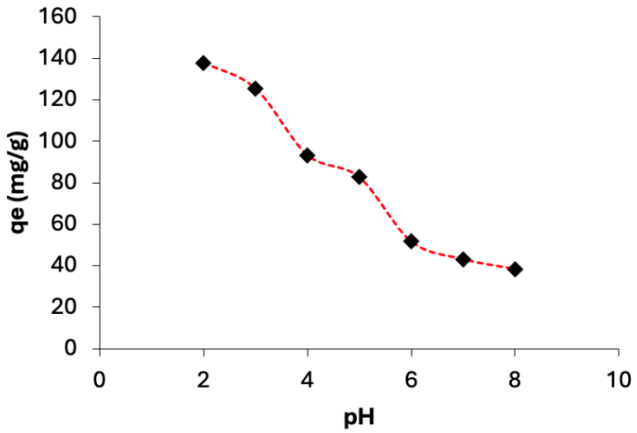

Figure 4. Effect of pH on Cr(VI) adsorption

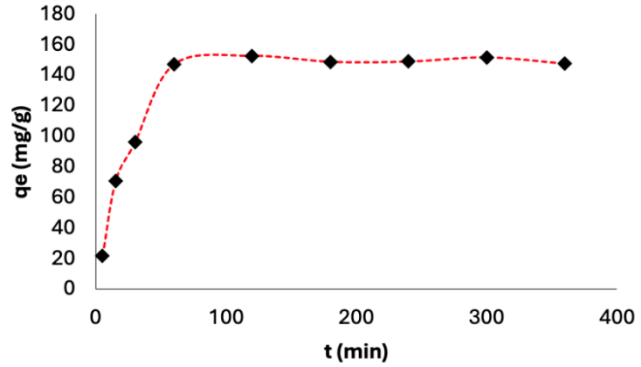

Figure 5. Effect of contact time on Cr(VI) adsorption

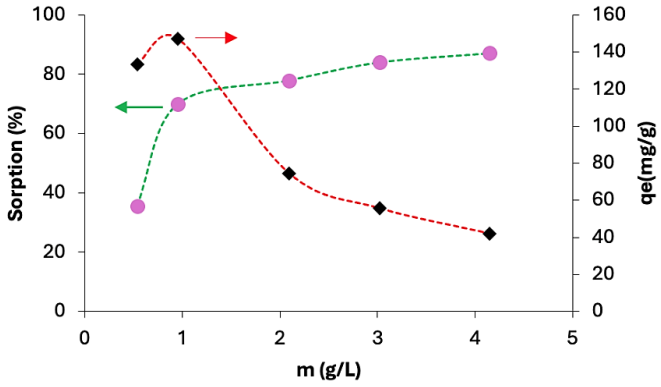

Figure 6. Effect of adsorbent dosage on Cr(VI) adsorption

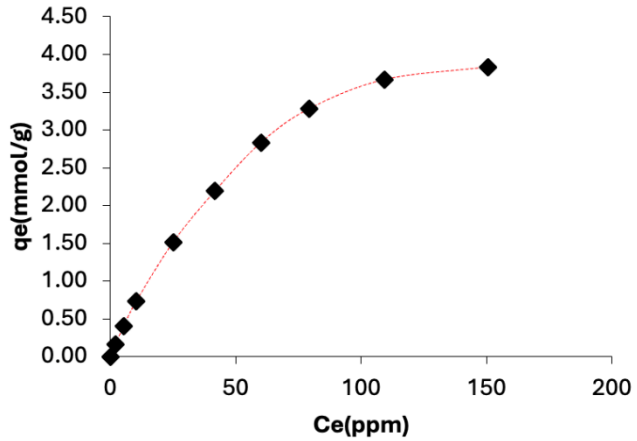

Figure 7. Effect of the initial Cr(VI) concentration on adsorption

3.5. Effect of contact time on adsorption of Cr (VI) ions

Contact time is a key factor in the adsorption process, with fast adsorption being a highly desirable trait. The impact of contact time on Cr(VI) adsorption was studied at intervals of 5, 15, 30, 60, 120, 180, 240, 300, and 360 minutes, using a composite dose of 1 g/L at pH 2 and a temperature of 25 °C. As illustrated in Fig. 5, the adsorption of Cr(VI) ions occurred rapidly as the contact time increased from 5 to 60 minutes, approaching equilibrium within this period. After 60 minutes, the adsorption rate slowed significantly with prolonged contact time. The equilibrium time is influenced by the type of adsorbent and the number of accessible active adsorption sites. The rapid adsorption efficiency of *n*Fe_3O_4-PPBC/Alg makes it cost-effective for use in small-scale reactor systems. Based on these findings, a contact time of 60 minutes was chosen as the optimum for future experiments.

3.6. Effect of adsorbent dose

The influence of adsorbent dosage on Cr(VI) removal was assessed through experiments conducted with various dosages (0.5, 1.0, 2.0, 3.0, and 4.0 g/L). Fig. 6 illustrates the relationship between adsorbent amounts and both adsorption capacity and removal efficiency. In general, the adsorption capacity of Cr(VI) initially increases with higher adsorbent doses but decreases after reaching a peak. Similarly, the percentage of Cr(VI) removal rises with the dose but levels off beyond a certain point. A rapid increase in Cr(VI) adsorption was observed when the *n*Fe_3O_4-PPBC/Alg dose was raised from 0.5 to 1.0 g/L. Beyond the 1 g/L dosage, adsorption reached a steady state, with only minor gains in efficiency. Adsorption capacity was found to increase proportionally with adsorbent dosage up to 1 g/L. Consequently, 1 g/L was identified as the optimal adsorbent dosage for further experiments.

3.7. Effect of the initial Cr(VI) concentration on adsorption

The initial concentration of Cr(VI) ions plays a crucial role as a driving force to counteract mass transfer resistances between the aqueous and solid phases. Higher removal efficiency results from the adsorbent's accessible active sites often capturing the majority of the Cr(VI) ions at lower starting concentrations. The adsorption rate decreases as the concentration rises because the active sites get saturated. Adsorption is stimulated by a larger concentration gradient, which is produced by higher starting concentrations. This may result in faster adsorption at first, but when adsorption sites are occupied, equilibrium is attained sooner. As the Cr(VI) concentration increases, the competition among

Cr(VI) ions for the limited adsorption sites becomes more intense, leading to a decline in the overall adsorption performance. Fig. 7 illustrates how the initial concentration affects adsorption. The adsorption capacity was measured across a range of initial Cr(VI) concentrations (10 to 350 ppm). Results indicated that adsorption capacity increased with higher Cr(VI) concentrations, up to a certain threshold. This enhancement in retention capacity with rising initial concentrations is likely due to the driving forces that help overcome the resistance encountered during the transfer of Cr(VI) ions from the solution to the nFe$_3$O$_4$-PPBC/Alg surface [23].

3.8. Adsorption isotherms

Adsorption isotherms illustrate the distribution of Cr(VI) ions between the liquid and solid phases once equilibrium is reached during the adsorption process [24]. Equilibrium data are crucial for analyzing and designing adsorption systems. The adsorption behavior of Cr(VI) on nFe$_3$O$_4$-PPBC/Alg was evaluated using widely recognized models, including the Langmuir, Freundlich, and Dubinin-Radushkevich (D-R) linearization methods to assess the composite's suitability. For the Langmuir model, two different linear methods were used, namely the Hanes-Woof and Scatchard methods [25]. The experimental isotherms for Cr(VI) adsorption onto nFe$_3$O$_4$-PPBC/Alg are presented in Fig. 8.

Based on equilibrium data, adsorption isotherms were analyzed, and R^2 values were calculated. The Langmuir model demonstrated the best fit to the data, with a correlation coefficient of 0.990, indicating a monolayer adsorption process. Considering the linear regression values in Table 1, the Langmuir model was found to be more suitable for describing the adsorption of Cr(VI). Accordingly, the Langmuir adsorption capacity was determined as Q_m=303.03 mg g^{-1}. The Langmuir isotherm model assumes that the adsorbent surfaces are homogeneous and form a single layer, with uniformly distributed and equivalent binding sites for Cr(VI) ions. This suggests that Cr(VI) ions are adsorbed onto nFe$_3$O$_4$-PPBC/Alg in a monolayer fashion. The separation factor (R_L) is a dimensionless constant derived from equilibrium parameters. If the R_L value lies between 0 and 1, the adsorption process is considered favorable for dye removal. For nFe$_3$O$_4$-PPBC/Alg, the R_L value was calculated to be 0.256, indicating that the adsorption of Cr(VI) ions onto this adsorbent is effective and suitable.

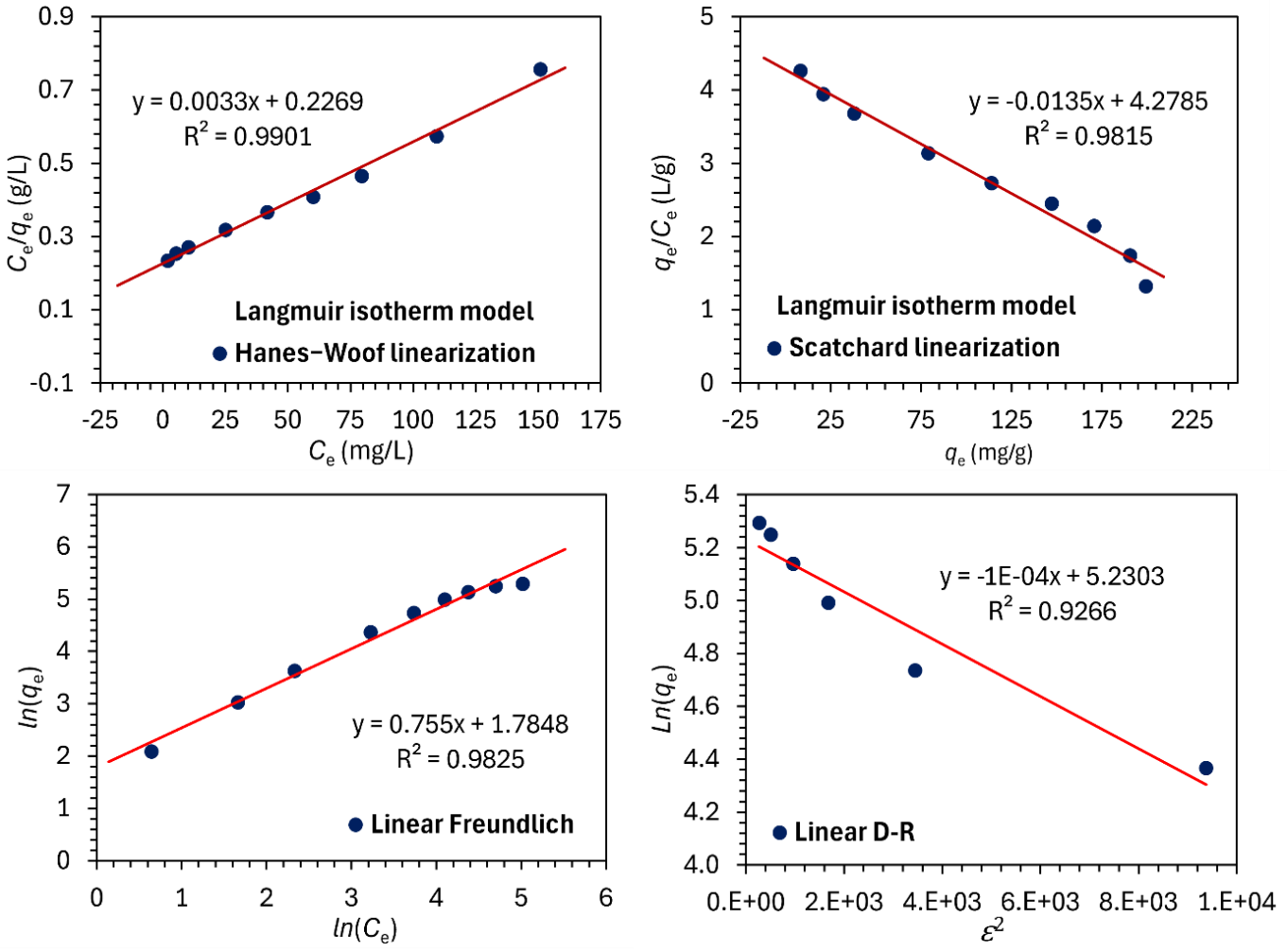

Figure 8. Langmuir (Hanes-Woof linearization), Langmuir (Scatchard linearization) Freundlich, and D-R isotherm graphs for nFe$_3$O$_4$-PPBC/Alg

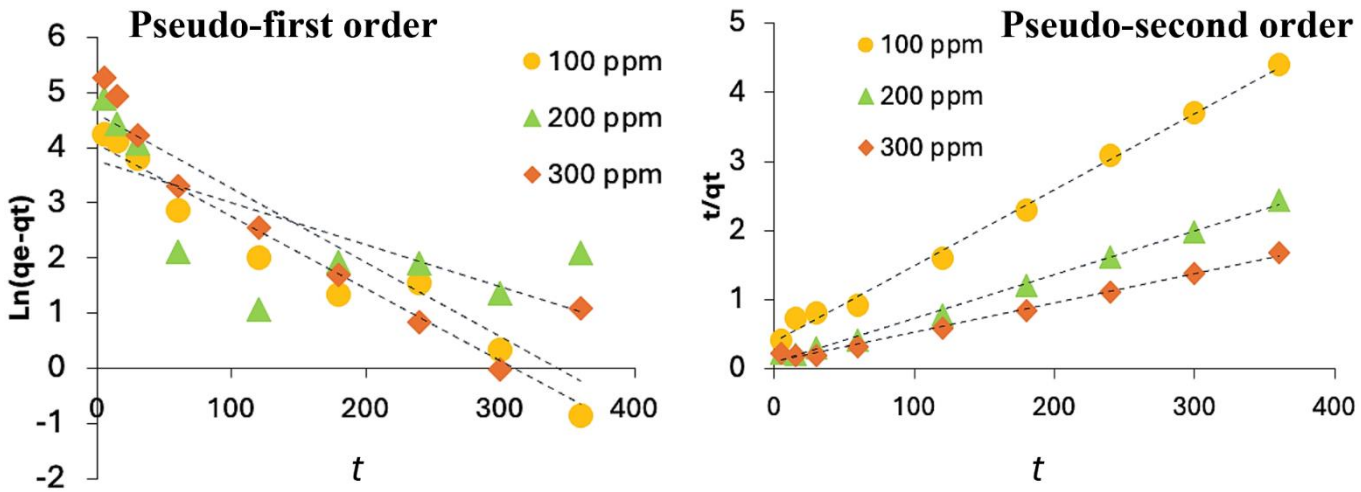

Figure 9. Plots of pseudo-first order and pseudo-second order kinetic models for Cr(VI) adsorption

The graph resulting from the application of the Freundlich equation to the data indicates that the adsorption of Cr(VI) does not follow this isotherm model (Fig. 8). The Freundlich isotherm is typically used for multilayer adsorption and assumes a heterogeneous surface where the heat of adsorption is distributed unevenly among the adsorbed molecules. The fact that the Cr(VI) adsorption by nFe$_3$O$_4$-PPBC/Alg does not align with the Freundlich model for single-layer adsorption further confirms this.

The Dubinin-Radushkevich (D-R) isotherm is widely used for systems where the adsorption curve is influenced by the sorbent's porous surface. This model helps identify whether the adsorption mechanism is physical or chemical. If the E value lies between 8 and 16 kJ/mol, the adsorption mechanism is considered chemical. E was calculated as 1.618 kj/mol in this study, thus, it can be said that the Cr(VI) adsorption mechanism proceeds physically (Table 1). The Scatchard plot, a linearized representation of the Langmuir isotherm, offers additional confirmation regarding the heterogeneity of binding sites. A linear plot suggests the presence of only one type of binding site, indicating homogeneity, whereas deviation from linearity implies heterogeneity. The R^2 value of 0.9815 demonstrates strong linearity, confirming the homogeneous nature of the surface and supporting the conclusion that the Langmuir model is the most suitable for describing the adsorption mechanism [25].

Additionally, the values obtained through Scatchard analysis align with the Langmuir isotherm, suggesting that the Langmuir adsorption isotherm is more appropriate for the process.

3.9. Adsorption kinetic modeling

The adsorption kinetics of Cr(VI) ions were analyzed using data fitted to pseudo-first order and pseudo-second order kinetic models (Fig. 9). The pseudo-second order model provided an excellent fit to the experimental data. A comparison between the experimental adsorption capacities and the theoretical values predicted by the two models is shown in Table 2. The theoretical q_e values from the first-order kinetic model deviated significantly from the experimental values, and the correlation coefficients were lower. This suggests that the first-order kinetic model does not adequately describe the adsorption of Cr(VI) by nFe$_3$O$_4$-PPBC/Alg. On the other hand, the correlation coefficients for the linear plots of t/q_t versus t in the second-order model were very close to 1. The theoretical q_e values in the second-order model were also very close to the experimental values, indicating that the second-order model fits the adsorption of Cr(VI) ions by nFe$_3$O$_4$-PPBC/Alg quite well.

Table 1. Values of isotherm parameters for Cr(VI) adsorption

Models	Linear equations	Parameters			
Langmuir	Hanes-Woof linearization $\frac{C_e}{q_e}=\frac{C_e}{Q_m}+\frac{1}{K_L Q_m}$	Q_m (mg/g) 301.25	K_L (L/mg) 0.0146	R^2 0.9901	R_L 0.256
	Scatchard linearization $\frac{q_e}{C_e}=Q_m K_L - q_e K_s$	Q_m (mg/g) 316.25	K_L (L/mg) 0.0135	R^2 0.9815	
Freundlich	$\ln q_e = lnK_F + \frac{1}{n} lnC_e$	K_F (L/g) 5.958	n 1.325	R^2 0.9825	
D-R	$lnq_e = lnQ_m - K_D\varepsilon^2$ $\varepsilon = RTln\left(1+\frac{1}{C_e}\right)$ $E=\frac{1}{\sqrt{2K_D}}$	Q_m (mg/g) 186.85	K_D (mol^2/kJ^2) 1.91×10^{-7}	E (kJ/mol) 1.618	R^2 0.9266

Table 2. Comparison of pseudo-first order and pseudo-second order adsorption rate constants, along with calculated and experimental q_e values, for various initial Cr(VI) concentrations.

		Pseudo-first order			Pseudo-second order		
C_o (mg/L)	$q_{e\ exp}$ (mg/g)	k_1 (min^{-1})	q_e (mg/g)	R^2	k_2 ($g.mg^{-1}.min^{-1}$)	q_e (mg/g)	R^2
100	82.34	0.0131	58.46	0.953	0.0003	90.91	0.996
200	155.57	0.0076	42.71	0.491	0.0004	158.73	0.995
300	217.91	0.0134	100.15	0.863	0.0002	238.10	0.993
Equations		$ln(q_e - q_t) = lnq_e - k_1 t$ Linear plot of $ln(q_e - q_t)$ vs. t			$\frac{t}{q_t} = \frac{1}{k_2 q_e^2} + \frac{1}{q_e} t$ Linear plot of t/q_t vs. t		

3.10. Thermodynamic parameters

The impact of temperature on Cr(VI) adsorption was examined over a range of temperatures (25 °C, 35 °C, 45 °C, and 55 °C) as shown in Fig. 10. At 25 °C, the negative value of the free energy change (ΔG°) indicates that the adsorption process occurs spontaneously, suggesting that *n*Fe_3O_4-PPBC/Alg is effective for Cr(VI) ion adsorption. The positive $\Delta H°$ value implies that the adsorption process is endothermic. Meanwhile, the positive $\Delta S°$ value indicates an increase in disorder at the adsorbent-Cr(VI) interface during the adsorption of Cr(VI) onto the surface of *n*Fe_3O_4-PPBC/Alg.

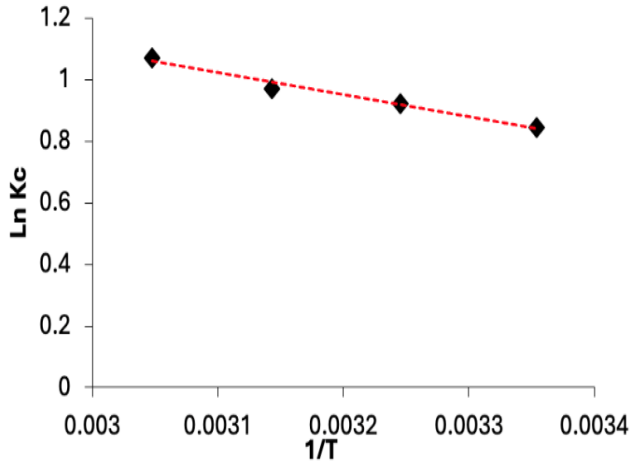

Figure 10. Plot of $ln(Kc) - 1/T$

3.11. Comparison of adsorbent capacities

Table 4 compares the adsorption capacities reported in the literature with those observed in our study. From the analysis of these studies, it can be concluded that *n*Fe_3O_4-PPBC/Alg exhibits a high adsorption capacity for Cr(VI) removal.

Table 3. Thermodynamic properties of Cr (VI) adsorption

$\Delta S°$	$\Delta H°$	$\Delta G°$ (J mol^{-1})				
(J $K^{-1}mol^{-1}$)	(J mol^{-1})	T=298 K	T=308 K	T=318 K	T=328 K	R^2
26.935	5 938.21	–2 092.39	–2 361.74	–2 631.08	–2 900.43	0.979

Table 4. Cr(VI) adsorbing capacities of different adsorbents

Adsorbent	q_e (mg/g)	Ref.
Calcium cross-linked Alginate/Chitosan biocomposite	9.8	
Iron cross-linked Alginate/Chitosan biocomposite	10.4	[5]
Zirconium cross-linked Alginate/Chitosan biocomposite	14.8	
Magnetic nano-hydroxyapatite encapsulated alginate beads	29.14	[26]
Magnetic alginate beads	14.29	[27]
Carbonized manganese-crosslinked Sodium alginate	104.50	[28]
Chitosan-humic acid-graphene oxide composite	83.64	[7]
Coffee grounds biochar/sodium alginate	30.66	[11]
Sugarcane bagasse biochar	15.73	
Brinjal stem biochar	71.89	[29]
Citrus peel biochar	16.34	
Cranberry kernel shell	6.81	
Rosehip seed shell	15.17	[24]
Banana peel	10.42	
nano-Fe_3O_4/pomegranate peel biochar/alginate beads	316.25	*This study*

3.12. Reusability study of *n*Fe_3O_4-PPBC/Alg composite

nFe_3O_4-PPBC/Algae composite for Cr(VI) removal must be regenerated and reused. For this purpose, 0.01M NaOH was employed in the desorption studies [30–32]. Fig. 11 displays the graph showing the data from repeated adsorption/desorption cycles for Cr(VI) ions after 7 cycles. The data from Fig. 11 reveal a slight decrease in the adsorption capacity of *n*Fe_3O_4-PPBC/Alg with each cycle. After 7 regeneration cycles, the Cr(VI) adsorption capacity of *n*Fe_3O_4-PPBC/Alg only decreased by 7.5%. These results suggest that *n*Fe_3O_4-PPBC/Alg can be effectively reused for Cr(VI) ion adsorption.

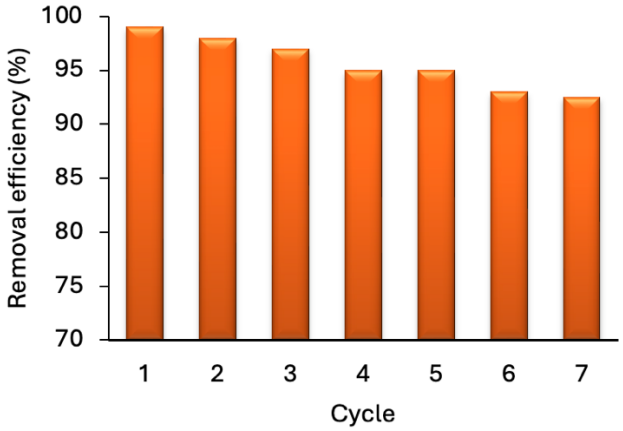

Figure 11. Reusability study of *n*Fe_3O_4-PPBC/Alg

4. Conclusions

In this study, *n*Fe_3O_4-PPBC/Alg was successfully synthesized using a straightforward method. The composite exhibited remarkable adsorption capacity, stability, and reusability, positioning it as a promising candidate for mitigating Cr(VI) pollution. The optimal reaction conditions were found to be an initial concentration of 2 mg/L, a pH of 2.0, an adsorbent dose of 1 g/L, and a reaction time of 60 minutes. The Langmuir

adsorption isotherm was found to be the most suitable for describing the observed adsorption phenomena, with the adsorption capacity of *n*Fe_3O_4-PPBC/Alg determined to be 316.25 mg/g for Cr(VI). The *n*Fe_3O_4-PPBC/Alg composite proves to be a highly effective for the removal of Cr (VI) from the aqueous medium. The combined effects of *nano*-Fe_3O_4, pomegranate peel biochar, and alginate enhance the adsorption process through various mechanisms such as electrostatic interactions, surface binding, and the availability of functional groups. Additionally, the use of *n*Fe_3O_4-PPBC/Alg adds a sustainable, cost-effective, and renewable component to the adsorbents. This research underscores the potential of such composite materials for treating industrial wastewater and highlights the significance of developing efficient, environmentally friendly adsorbent for sustainable environmental cleanup.

References

[1] S. Dutta, R.K. Sharma, Sustainable magnetically retrievable nanoadsorbents for selective removal of heavy metal ions from different charged wastewaters, Sep Sci Technol, 11, 2019, 371–416.

[2] J. Niu, P. Ding, X. Jia, G. Hu, Z. Li, Study of the properties and mechanism of deep reduction and efficient adsorption of Cr (VI) by low-cost Fe_3O_4-modified ceramsite, Sci Total Environ, 688, 2019, 994–1004.

[3] K. Staszak, I. Kruszelnicka, D. Ginter-Kramarczyk, W. Góra, M. Baraniak, G. Lota, M. Regel-Rosocka, Advances in the removal of Cr (III) from spent industrial effluents—A review, Materials, 16(1), 2022, 378.

[4] D. Lohan, R. Jain, A. Srivastava, S. Dutta, D. Mohan, R.K. Sharma, Surface engineering approaches for the design of magnetic biochar-composites for removal of heavy metals: a comprehensive review, J Environm Chem Eng, 2023, 111448.

[5] G. Venkatrajan, J. Venkatesan, N. Madankumar, S. Pushparaju, Effective chromium removal of metal anchored alginate-chitosan binary bio-composites. Int J Biol Macromol, 264, 2024, 130408.

[6] J. Bajpai, R. Shrivastava, A.K. Bajpai, Dynamic and equilibrium studies on adsorption of Cr (VI) ions onto binary bio-polymeric beads of cross linked alginate and gelatin, Colloids Surf A: Physicochem Eng Asp, 236(1-3), 2004, 81–90.

[7] Ş. Parlayıcı, A. Avcı, E. Pehlivan, Fabrication of novel chitosan-humic acid-graphene oxide composite to improve adsorption properties for Cr (VI), Arab J Geosci, 12, 2019,1–13.

[8] P. Chen, R. Cheng, G. Meng, Z. Ren, J. Xu, P. Song, H. Wang, L. Zhang, Performance of the graphite felt flow-through electrode in hexavalent chromium reduction using a single-pass mode, J Hazard Mater, 416, 2021, 125768.

[9] Y. Liu, X. Ke, X. Wu, C. Ke, R. Chen, X. Chen, X. Zheng, Y. Jin, B. Van der Bruggen, Simultaneous removal of trivalent chromium and hexavalent chromium from soil using a modified bipolar membrane electrodialysis system, Environ Sci Technol, 54(20), 2020, 13304–13313.

[10] A. Kuanar, S.K. Kabi, M. Rath, N.K. Dhal, R. Bhuyan, S. Das, D. Kar, A comparative review on bioremediation of chromium by bacterial, fungal, algal and microbial consortia, Geomicrobiol J, 39(6), 2022, 515–530.

[11] Y. Tian, X. Sun, N. Chen, X. Cui, H. Yu, Y. Feng, D. Xi, W. He, Efficient removal of hexavalent chromium from wastewater using a novel sodium alginate-biochar composite adsorbent, J Water Process Eng, 64, 2024, 105655.

[12] B. Devi, M. Goswami, A. Devi, Entrapment behaviours of trivalent and hexavalent chromium from aqueous medium using edible alkali-derived activated carbon of Eichhornia crassipes (water hyacinth), Environ Sci Pollut Res, 31(4), 2024, 6025–6039.

[13] Ş. Parlayıcı, E. Pehlivan, An ecologically sustainable specific method using new magnetic alginate-biochar from acorn cups (Quercus coccifera L.) for decolorization of dyes, Polymer Bull, 80(10), 2023, 11167–11191.

[14] L. Li, Q. Liao, B. Hou, C. He, J. Liu, B. Li, M. Yu, Y. Liu, B. Lai, B. Yang, Synchronous reduction and removal of hexavalent chromium from wastewater by modified magnetic chitosan beads, Sep Purif Technol, 304, 2023, 122363.

[15] Q. Feng, B. Wang, M. Chen, P. Wu, X. Lee, Y. Xing, Invasive plants as potential sustainable feedstocks for biochar production and multiple applications: a review, Resour Conserv Recycl, 164, 2021, 105204.

[16] C. Zhao, B. Wang, B.K.G. Theng, P. Wu, F. Liu, S. Wang, X. Lee, M. Chen, L. Li, X. Zhang, Formation and mechanisms of nano-metal oxide-biochar composites for pollutants removal: a review, Sci Total Environ, 767, 2021, 145305.

[17] S. Fan, J. Zhou, Y. Zhang, Z. Feng, H. Hu, Z. Huang, Y. Qin, Preparation of sugarcane bagasse succinate/alginate porous gel beads via a self-assembly strategy: Improving the structural stability and adsorption efficiency for heavy metal ions, Bioresour Technol, 306, 2020, 123128.

[18] Y. He, J. Chen, J. Lv, Y. Huang, S. Zhou, W. Li, Y. Li, F. Chang, H. Zhang, T. Wagberg, G. Hu, Separable amino-functionalized biochar/alginate beads for efficient removal of Cr (VI) from original electroplating wastewater at room temperature, J Clean Product, 373, 2022, 133790.

[19] R. Sun, S. Gao, K. Zhang, W. T. Cheng, G. Hu, Recent advances in alginate-based composite gel spheres for removal of heavy metals, Int J Biol Macromol, 2024, 131853.

[20] R. Wen, B. Tu, X. Guo, X. Hao, X. Wu, H. Tao, An ion release controlled Cr (VI) treatment agent: Nano zero-valent iron/carbon/alginate composite gel, Int J Biol Macromol, 146, 2020, 692–704.

[21] A. F. Hassan, A. M. Abdel-Mohsen, H. Elhadidy, Adsorption of arsenic by activated carbon, calcium alginate and their composite beads, Int J Biol Macromol, 68, 2014, 125–130.

[22] F. Amalina, A.S. Abd Razak, S. Krishnan, A.W. Zularisam, M. Nasrullah, A comprehensive assessment of the method for producing biochar, its characterization, stability, and potential applications in regenerative economic sustainability–a review, Clean Mater, 3, 2022, 100045.

[23] B.H. Hameed, A.A. Ahmad, Batch adsorption of methylene blue from aqueous solution by garlic peel, an agricultural waste biomass, J Hazard Mater, 164(2-3), 2009, 870–875.

[24] Ş. Parlayici, E. Pehlivan, Comparative study of Cr (VI) removal by bio-waste adsorbents: equilibrium, kinetics, and thermodynamics, J Anal Sci Technol, 10(1), 2019, 1–8.

[25] A.P. Mikolajczyk, D.L.B. Fortela, J.C. Berry, W.M. Chirdon, R.A. Hernandez, D.D. Gang, M.E. Zappi, Evaluating the suitability of linear and nonlinear regression approaches for the Langmuir adsorption model as applied toward biomass-based adsorbents: Testing residuals and assessing model validity, Langmuir 2024, 40(39), 20428–20442.

[26] S. Periyasamy, V. Gopalakannan, N. Viswanathan, Hydrothermal assisted magnetic nano-hydroxyapatite encapsulated alginate beads for efficient Cr (VI) uptake from water, J Environ Chem Eng, 6(1), 2018, 1443–1454.

[27] V. Gopalakannan, N. Viswanathan, Synthesis of magnetic alginate hybrid beads for efficient chromium (VI) removal, Int J Biol Macromol, 72, 2015, 862–867.

[28] W. Mao, L. Zhang, Y. Zhang, Y. Wang, N. Wen, Y. Guan, Adsorption and photocatalysis removal of arsenite, arsenate, and hexavalent chromium in water by the carbonized composite of

manganese-crosslinked sodium alginate, Chemosphere, 292, 2022, 133391.

[29] H. Chaudhary, K. S. Rao, Impact of biochar produced at different pyrolysis conditions on heavy metal contaminated soil, Environ Geochem Health, 46(9), 2024, 307.

[30] Y. Cao, J. Huang, X. Peng, D. Cao, A. Galaska, S. Qiu, J. Liu, M.A. Khan, D. Young, J.E. Ryu, H. Feng, N. Yerra, Z. Guo, Poly (vinylidene fluoride) derived fluorine-doped magnetic carbon nanoadsorbents for enhanced chromium removal, Carbon, 115, 2017, 503–514.

[31] J. Wang, K. Pan, Q. He, B. Cao, Polyacrylonitrile/polypyrrole core/shell nanofiber mat for the removal of hexavalent chromium from aqueous solution, J Hazard Mater, 244, 2013, 121–129.

[32] C. Luo, Z. Tian, B. Yang, L. Zhang, S. Yan, Manganese dioxide/iron oxide/acid oxidized multi-walled carbon nanotube magnetic nanocomposite for enhanced hexavalent chromium removal, Chem Eng J, 234, 2013, 256–265.